npj | spintronics

www.nature.com/npjspintronics

ARTICLE OPEN

Check for updates

Energetic perspective on emergent inductance exhibited by magnetic textures in the pinned regime

Soju Furuta[1], Samuel Harrison Moody[2], Kyohei Kado[3], Wataru Koshibae[4] and Fumitaka Kagawa[1,4]✉

Spatially varying magnetic textures can exhibit electric-current-induced dynamics as a result of the spin-transfer torque effect. When such a magnetic system is electrically driven, an electric field is generated, which is called the emergent electric field. In particular, when magnetic-texture dynamics are induced under the application of an AC electric current, the emergent electric field also appears in an AC manner, notably, with an out-of-phase time profile, thus exhibiting inductor behavior, often called an emergent inductor. Here we show that the emergent inductance exhibited by magnetic textures in the pinned regime can be explained in terms of the current-induced energy stored in the magnetic system. We numerically find that the inductance values defined from the emergent electric field and the current-induced magnetization-distortion energy, respectively, are in quantitative agreement in the so-called adiabatic limit. Our findings indicate that emergent inductors retain the basic concept of conventional inductors; that is, the energy is stored under the application of electric current.

npj Spintronics (2023)1:1 ; https://doi.org/10.1038/s44306-023-00004-1

INTRODUCTION

Strong coupling between conduction-electron spin and underlying spin texture forms the basis of rich phenomena, such as electric-current-induced dynamics of the spin system via the spin-transfer-torque (STT) effect[1–3] and the spin-dynamics-induced electromotive force (spin motive force or emergent-electric field (EEF))[4–8]. Although obtaining a general expression for the EEF is difficult, a concise form is available for a specific situation; that is, the magnetic texture is slowly varying in space, and the conduction-electron spins are always parallel to the local magnetic moments of the magnetic texture. In this limit, often referred to as the adiabatic limit, electron transport under the influence of the magnetic texture is described by introducing the effective U(1) gauge field, which results in the emergent magnetic field and EEF[4]. The EEF, which is the focus of this study, can be described in the following equation[4,5]:

$$e_i(\boldsymbol{r},t) = \frac{\hbar}{2|e|}\boldsymbol{m}(\boldsymbol{r},t)\cdot[\partial_i\boldsymbol{m}(\boldsymbol{r},t)\times\partial_t\boldsymbol{m}(\boldsymbol{r},t)], \tag{1}$$

where $e(>0)$ is the elementary charge, $\boldsymbol{m}(\boldsymbol{r},t)$ is the unit vector of the local magnetic moment at position $\boldsymbol{r}$ and time t, and ∂_i $(i=x,y,z)$ and ∂_t denote the spatial and time derivatives, respectively. When the conduction-electron spins are not fully polarized, the so-called spin-polarization factor P is further considered for the resulting electric field[5,8]. As explicitly expressed in this equation, the EEF can appear only when the magnetic texture is time evolving.

Recently, the interplay between the STT and EEF has attracted much attention as a source of a new class of inductors, often called an emergent inductor[9–14]. To understand the emergent inductor under the application of an AC electric current, it is still instructive to consider the dynamics of a magnetic system under a DC electric current. In the following, we focus on the so-called pinned regime[15–17], in which a magnetic system does not exhibit a steady flow under a DC electric current[18–24]. When a DC current (let j be the current density) is applied, a magnetic texture starts to deform as a result of the STT effect, but its dynamics are only transient and eventually stop at $t\to\infty$ by definition of the pinned regime; thus, $\partial_t\boldsymbol{m}=0$ at the final state, and hence, no EEF appears: We will illustrate the case of a helical magnetic texture in the Results section. In the linear-response regime, the change in the local magnetization direction at the final state, $\delta\boldsymbol{m}$, is elastic and proportional to j; i.e., $\delta\boldsymbol{m}\propto j$.

The situation under an AC electric current, $j(t)=j_0\sin\omega t$, can be considered in a similar way. As long as the linear and low-frequency response regimes are considered, $\delta\boldsymbol{m}(t)$ is proportional to the instantaneous value of $j(t)$. In this limit, the magnetization has an in-phase response to the applied AC current: $\delta\boldsymbol{m}(t)\propto j(t)=j_0\sin\omega t$. Note that as a natural consequence of the application of an AC current, the current-induced dynamics persist, and thus $\partial_t\delta\boldsymbol{m}$ remains finite even in the pinned regime; $\partial_t\delta\boldsymbol{m}\propto j_0\omega\cos\omega t=\mathrm{d}j(t)/\mathrm{d}t$, and this is an out-of-phase response to the applied AC current. Thus, an out-of-phase linear-response EEF can appear because $\boldsymbol{m}\cdot(\partial_i\boldsymbol{m}\times\partial_t\delta\boldsymbol{m})$ is finite, and it is expressed as

$$e_i(t)=\tilde{L}\frac{\mathrm{d}j(t)}{\mathrm{d}t}, \tag{2}$$

where $\tilde{L}$ is a normalized inductance (the unit is Henry meter, H m, which we may term "inductivity", in analogy to the terminology of resistivity) defined in the linear-response and low-frequency regimes. By multiplying the sample length ℓ with both sides of Eq. (2) and inserting $I=Aj$, where I and A, respectively, represent the applied current and the sample cross-section area, one can obtain a standard equation describing the self-induction phenomenon:

$$V=L\frac{\mathrm{d}I}{\mathrm{d}t}, \tag{3}$$

where $L\equiv\tilde{L}(\ell/A)$ and V represents the self-induction coefficient and the inductive counter-electromotive force, respectively. This voltage-current relation in the inductor defines L. In general, L is frequency dependent and may be represented by a complex

[1]Department of Physics, Tokyo Institute of Technology, Tokyo 152-8551, Japan. [2]Durham University, Centre for Materials Physics, Durham DH1 3LE, UK. [3]Department of Applied Physics, The University of Tokyo, Tokyo 113-8656, Japan. [4]RIKEN Center for Emergent Matter Science (CEMS), Wako 351-0198, Japan. ✉email: kagawa@phys.titech.ac.jp

number, $L^*(\omega)$, the imaginary part of which describes the phase delay of the voltage response from d*I*/d*t*.

Nevertheless, as long as one considers the low-frequency regime such that $\mathrm{Re}\,L^*(\omega) \gg \mathrm{Im}\,L^*(\omega)$ is satisfied, the inductance can be taken as a constant real number. In this case, the electric work required to supply a current to the inductor (assume $I = 0$ for $t \le 0$) is calculated from Eq. (3) as follows:

$$\begin{aligned}\int_0^t \mathrm{d}t' I(t')V(t') &= \int_0^t \mathrm{d}t' \frac{\mathrm{d}}{\mathrm{d}t'}\left(\frac{1}{2}LI(t')^2\right)\\ &= \frac{1}{2}LI(t)^2.\end{aligned} \tag{4}$$

This electric work, $\frac{1}{2}LI(t)^2$, should be positive, and as is clear from the derivation, it is nondissipative in nature; thus, given energy conservation, the corresponding energy can be viewed as stored in the inductor in the circuit. Alternatively, the electric work done by the external power supply can also be viewed as stored in the energy of the whole system; thus, the energy increase of the whole system, $\Delta E_{\mathrm{system}}(I(t))$, satisfies $\Delta E_{\mathrm{system}}(I(t)) = \frac{1}{2}LI(t)^2$.

In a classical inductor made of a coil, it can be shown analytically that $\Delta E_{\mathrm{system}}(t)$ is equal to the magnetic-field energy, $\frac{1}{2}\int \mathrm{d}V \boldsymbol{H}(t)\cdot\boldsymbol{B}(t)$. Thus, at least for the case of the classical inductors, the value of L in the low-frequency regime can be defined in two ways: One is from the electric response due to the electromagnetic induction (EMI), and L_{EMI} is given by $V(t) = L_{\mathrm{EMI}}\frac{\mathrm{d}I(t)}{\mathrm{d}t}$; the other is from the energy increase of the whole system, and L_{energy} is given by $\Delta E_{\mathrm{system}}(t) = \frac{1}{2}L_{\mathrm{energy}}I(t)^2$. Although the two definitions of L are based on different perspectives, they result in the same value, $L_{\mathrm{EMI}} = L_{\mathrm{energy}}$.

In the case of emergent inductors, the microscopic mechanism is based on quantum mechanics, and it is thus quite different from that of classical inductors. Nevertheless, Eq. (3) remains valid for describing the electric response of emergent inductors, and energy conservation should invariably hold. Therefore, it is expected that the value of L of the emergent inductor in the low-frequency regime can be defined also in terms of $\Delta E_{\mathrm{system}}$. However, to the best of the authors' knowledge, the emergent inductance has never been discussed from such an energetic perspective, although the energetic implications of Eq. (1) have been discussed by Barnes and Maekawa[5].

In this paper, we address this issue numerically using micromagnetic software. We consider a magnetic system in a pinned regime and perform micromagnetic simulations for the current-induced dynamics of a magnetic texture; then, we calculate the time evolutions of the voltage due to EEF, $V_{\mathrm{e}}(t)$, and the energy increase of the magnetic system, $\Delta E(t)$, according to Eq. (1) and our model spin-Hamiltonian (see below), respectively. We can thus numerically derive L_{EMI} and L_{energy} and, by comparing the two values, test the energetic perspective on the emergent inductor.

By investigating the energetic perspective, we also aim to gain insight into the meaning of negative emergent inductance, an intriguing issue reported in past experimental studies[10,11,14] and theoretical studies[12,13]. The term "negative inductance" immediately evokes many questions: Is the negative emergent inductor really stable, even though the negative inductance is known to be unstable (Supplementary Note 1)? Similarly, does the negative inductance mean that the current-supplied state of the material has a lower energy than that of the zero-current state? Or does the emergent inductance no longer have an energetic meaning, even though electrodynamics textbooks state that the energy definition is fundamental for inductance[25]? It is known that complex impedance at low frequencies can be analyzed by assuming an appropriate equivalent circuit consisting of positive, real-valued circuit elements, R (resistance), L (inductance), and C (capacitance). However, in what cases does negative L need to be introduced beyond this well-established framework? Since these fundamental questions remain unanswered, the physical meaning of the negative inductance remains unclear.

RESULTS

Models

Simulating an emergent inductance using micromagnetic software has the following limitations. First, in calculating the magnetic-texture dynamics under the electric current and resulting EEF, we should take the spatial derivative of the magnetic texture, $\partial_i \boldsymbol{m}(\boldsymbol{r})$. It follows that, for our approach to be valid, the magnetic texture that we consider should be slowly varying in space. To minimize this problem, in this study, we restrict ourselves to long-period helical magnetic textures.

Second, although the real system is ultimately an electron-spin-coupled system, we consider a Hamiltonian and an equation of motion, both of which describe the magnetic subsystem only. Thus, we can calculate the current-induced energy increase $\Delta E(t)$ only for the local magnetic moments, which is not, strictly speaking, equal to $\Delta E_{\mathrm{system}}(t)$ when an energy increase in the electronic subsystem is not negligible.

Third, our calculation of the EEF is based on Eq. (1). As long as a slowly varying magnetic texture is considered, one can describe electron transport properties by introducing a gauge field, which has in general SU(2) symmetry[22]. By taking the adiabatic limit, the SU(2) gauge field reduces to a U(1) gauge field: Eq. (1) is thus derived. Conversely, when the system deviates from the adiabatic limit, the use of Eq. (1) becomes less justified.

Note that the first issue is, in principle, avoidable by considering a sufficiently slowly varying magnetic texture and increasing numerical efforts. In contrast, the other two issues are more fundamental and thus unavoidable as long as the approach is based on the spin-only Hamiltonian and Eq. (1), which is the formalism for the adiabatic limit.

In this study, we consider long-period helical magnetic textures that are stabilized by the Dzyaloshinskii–Moriya (DM) interaction. We consider both a clean system without any disorder and dirty systems including randomly distributed disorder. Our model Hamiltonian is:

$$\begin{aligned}\mathscr{H} = &\int \frac{\mathrm{d}^3 r}{a^3}\left[\frac{J}{2}(\nabla \boldsymbol{m})^2 + D\boldsymbol{m}\cdot(\nabla\times\boldsymbol{m})\right]\\ &-\sum_{k\in\Lambda}\int_{V_k}\mathrm{d}^3 r\, K_{\mathrm{imp}}(\boldsymbol{m}_k\cdot\boldsymbol{n}_{\mathrm{imp},k})^2\end{aligned} \tag{5}$$

where J is the exchange stiffness, D is the DM interaction and a is the lattice constant. When examining a randomness effect, we introduce the last term of Eq. (5): $K_{\mathrm{imp}}(>0)$ represents the magnetic-easy-axis anisotropy along a randomly chosen direction, $\boldsymbol{n}_{\mathrm{imp},k}$, at the kth cell (the cell volume V_k is 3^3 nm^3), and Λ is a set of random numbers.

When simulating the current-induced dynamics of a given helical magnetic structure, we insert the spin Hamiltonian into the following Landau–Lifshitz–Gilbert (LLG) equation[26]:

$$\begin{aligned}\frac{\mathrm{d}\boldsymbol{m}_{\boldsymbol{r}}(t)}{\mathrm{d}t} = &-\frac{\gamma}{1+\alpha^2}\frac{\mathrm{d}\mathscr{H}}{\mathrm{d}\boldsymbol{m}_{\boldsymbol{r}}}\times\boldsymbol{m}_{\boldsymbol{r}} - \frac{\alpha\gamma}{1+\alpha^2}\left[\boldsymbol{m}_{\boldsymbol{r}}\times\left(\frac{\mathrm{d}\mathscr{H}}{\mathrm{d}\boldsymbol{m}_{\boldsymbol{r}}}\times\boldsymbol{m}_{\boldsymbol{r}}\right)\right]\\ &+\frac{1}{1+\alpha^2}\{(1+\beta\alpha)\boldsymbol{m}_{\boldsymbol{r}}\times[\boldsymbol{m}_{\boldsymbol{r}}\times(\boldsymbol{u}\cdot\nabla)\boldsymbol{m}_{\boldsymbol{r}}]\\ &+(\beta-\alpha)[\boldsymbol{m}_{\boldsymbol{r}}\times(\boldsymbol{u}\cdot\nabla)\boldsymbol{m}_{\boldsymbol{r}}]\},\end{aligned} \tag{6}$$

where $\boldsymbol{u}$ represents the spin drift velocity, α is the Gilbert damping constant, β is a dimensionless constant that characterizes the nonadiabatic electron spin dynamics, and $\gamma(>0)$ is the gyromagnetic ratio; $\boldsymbol{u}$ is related to the electric current density $\boldsymbol{j}$ by $\boldsymbol{u} = \frac{P\mu_{\mathrm{B}}}{2eM_{\mathrm{s}}(1+\beta^2)}\boldsymbol{j}$, where μ_{B} is the Bohr magneton and M_{s} is the saturation magnetization. When implementing the micromagnetic

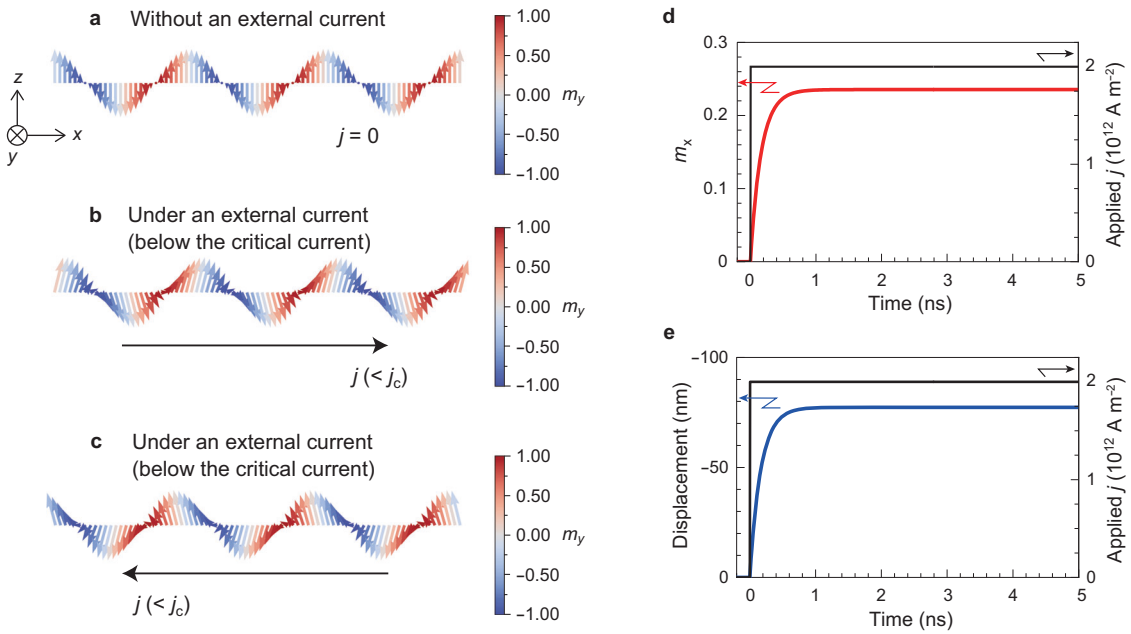

Fig. 1 Schematics for a helical magnetic texture and its distortion under the application of an electric current. a Pristine helical magnetic structure with right-handed chirality under zero electric current. **b**, **c** Illustration of the current-induced distortion of the helical magnetic structure under rightward (**b**) and leftward (**c**) electric currents at steady state. **d** Time profile of m_x under a DC current application. The tilting direction of helical magnetism shown in **b** and **c** is reversed for a helical magnetic structure with left-handed chirality (not shown). **e** Time profile of the translational displacement, which is defined with respect to the position at which the local moment exhibits the maximum m_z. In **b**–**e**, a relatively large current density, 2.0×10^{12} A m^{-2}, is used to obtain a large distortion, just for clarity, but it is still lower than the critical current density, $\approx 5.0 \times 10^{12}$ A m^{-2}. In the present case, m_x is uniform in space.

simulation, we use the open software MuMax3 (https://mumax.github.io/download.html)[27]. We choose the following parameter set: $J/(2a^3) = 1.8 \times 10^{-11}$ J m^{-1}, $D/a^3 = 2.8 \times 10^{-3}$ J m^{-2}, $K_{\rm imp} = 1.0 \times 10^6$ J m^{-3}, $M_{\rm s} = 2.45 \times 10^5$ A m^{-1}, $P = 1$, and $\alpha = 0.04$. In the following simulation, we apply a current density of a sufficiently small magnitude so that the magnetic system is certainly in a pinned regime.

As shown below, we find that with respect to the input AC electric current, $j(t) = j_0 \sin \omega t$, the output AC emergent voltage, $V_{\rm e}(t)$ is $\propto j_0 \omega \cos \omega t$, and the time-evolving energy-increase of the magnetic system, $\Delta E(t)$ is $\propto (j_0 \sin \omega t)^2$. From these observations, $L_{\rm EMI}$ and $L_{\rm energy}$ are derived from the following equations:

$$V_{\rm e}(t) = \langle e_x(t) \rangle \ell = L_{\rm EMI} \frac{{\rm d}I(t)}{{\rm d}t} = \left(\tilde{L}_{\rm EMI} \frac{\ell}{A} \right) \frac{{\rm d}I(t)}{{\rm d}t}, \tag{7}$$

$$\Delta E(t) = \frac{1}{2} L_{\rm energy} I(t)^2 = \frac{1}{2} \left(\tilde{L}_{\rm energy} \frac{\ell}{A} \right) I(t)^2, \tag{8}$$

where $\langle \cdots \rangle$ denotes a spatially averaged value.

Clean systems

As one of the simplest systems, we first study the following quasi-one-dimensional system: the system size is $243 \times 18 \times 1$ ($\ell = 243 \times 3$ nm and $A = 18 \times 1 \times 3^2$ nm^2) under the periodic boundary condition, including no disorder. In such a clean system, the spin system exhibits a pristine helical structure with the yz helical plane (Fig. 1a, which illustrates the case of right-handed chirality). When $\beta = 0$ in Eq. (6) and the electric current is below a threshold value (in the present system, $\approx 5.0 \times 10^{12}$ A m^{-2}), the spin system is in the so-called intrinsic pinning regime[19,21,22]; namely, when a DC current is applied at $t = 0$, the helical texture starts to deform along the current direction, and after ~1 ns, static and elastic tilting along the x direction is realized, forming a conical state with a net magnetization (Fig. 1b–d): In addition, the position at which the local magnetic moment exhibits the maximum m_z is slightly displaced and stopped (Fig. 1e). In contrast, when β is finite, the helical texture exhibits a steady flow for arbitrary small current density because of the absence of any disorder[18,19,24], and thus in the clean system, the magnetic-texture dynamics in a pinned regime, which is a focus of this study, is realized only when $\beta = 0$. When an AC electric current is applied, magnetic moment tilting occurs within the pinned regime toward the $+x$ and $-x$ directions alternatingly with time, yielding an alternating electric field according to Eq. (1).

For such a pristine helical magnetic texture, the current-induced dynamics in the pinned regime can be analytically derived within the framework of Eq. (6) with $\beta = 0$. Thus, assuming Eq. (1) for the EEF, the microscopic expression for $L_{\rm EMI}$ can be derived as reported in previous theoretical studies[9,12] (see also Supplementary Note 2). The result is

$$L_{\rm EMI} = \left(\frac{P\hbar}{2|e|} \right)^2 \frac{a^3}{J} \frac{\ell}{A} = \tilde{L}_{\rm EMI} \frac{\ell}{A}. \tag{9}$$

Similarly, the energy increase, ΔE, can also be derived (for the derivation, see Supplementary Note 2); then, by assuming the energy conservation ($\Delta E = \frac{1}{2} L_{\rm energy} I^2$), the expression of $L_{\rm energy}$ can be obtained:

$$L_{\rm energy} = \left(\frac{P\hbar}{2|e|} \right)^2 \frac{a^3}{J} \frac{\ell}{A} = \tilde{L}_{\rm energy} \frac{\ell}{A}. \tag{10}$$

Thus, we find $\tilde{L}_{\rm EMI} = \tilde{L}_{\rm energy}$ analytically for the case of the intrinsically pinned helical magnetic texture ($\beta = 0$). This agreement means that the energy increase of the magnetic system is equal to the work done by the external power supply against the inductive counter-electromotive force due to the EEF, and is consistent with the first law of thermodynamics. By substituting $J/(2a^3) = 1.8 \times 10^{-11}$ J m^{-1} into Eqs. (9) or (10), we obtain $\tilde{L} = 3.006 \times 10^{-21}$ H m. This value can be used to test the validity and accuracy of our numerical approach.

To numerically derive the value of the emergent inductance, we calculate $V_{\rm e}(t)$ and $\Delta E(t)$ for the AC current-induced helical-texture

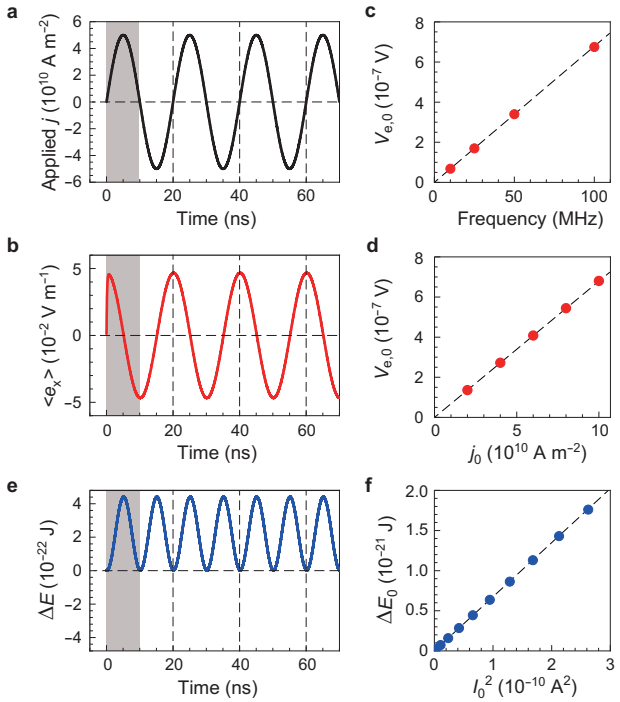

Fig. 2 Electric and energetic responses emerging from AC-current-induced dynamics of the helical magnetic texture. **a**, **b** Time profiles of the applied AC current (**a**) and resulting emergent electric field (**b**). **c**, **d** Frequency (**c**) and current amplitude (**d**) dependence of the amplitude of the emergent electric field. **e** Time profile of the energy increase of the magnetic system. **f** Amplitude of the oscillating magnetic-system energy as a function of current square, I_0^2. In **a**, **b**, **e** the data in the first half cycle (gray hatched) are excluded from the analysis to analyze a system that is sufficiently settled for a steady-state cycle under an AC current. These results are obtained in the clean system, and the qualitatively same results are also obtained in the dirty systems.

dynamics. When $j(t) = j_0 \sin \omega t$ with $j_0 = 5.0 \times 10^{10}$ A m^{-2} and $\omega/2\pi = 50$ MHz is applied (Fig. 2a), the emergent voltage exhibits $V_e(t) = V_{e,0} \cos \omega t$ (Fig. 2b). We further confirm that $V_{e,0}$ is proportional to both ω and j_0 (Fig. 2c and d, respectively). These observations are consistent with the behavior expressed by Eq. (7), representing a numerical demonstration of the emergent inductor consisting of a helical magnetic structure. We also find that $\Delta E(t)$ changes according to $\Delta E(t) = \Delta E_0 \sin^2 \omega t$ (Fig. 2e), and the amplitude ΔE_0 is proportional to $I_0^2 = (Aj_0)^2$ (Fig. 2f), consistent with $\Delta E(t) \propto j(t)^2$, as expressed by Eq. (8). From these behaviors, we obtain $\tilde{L}_{\rm EMI} = 2.98 \times 10^{-21}$ H m and $\tilde{L}_{\rm energy} = 2.96 \times 10^{-21}$ H m. The relative error δ, defined by $\delta = |\tilde{L}_{\rm EMI} - \tilde{L}_{\rm energy}|/\tilde{L}_{\rm energy}$, is <1%, leading us to conclude that $\tilde{L}_{\rm EMI} = \tilde{L}_{\rm energy}$ is confirmed within the numerical error. Furthermore, these numerical results have an error of <2% within the theoretical value, $\tilde{L} = 3.006 \times 10^{-21}$ H m, supporting the validity of our numerical approach.

Dirty systems

To see the universality of $L_{\rm EMI} = L_{\rm energy}$, it is helpful to numerically examine disordered helical textures in dirty systems. To this end, we prepare a two-dimensional system (the system size is $243 \times 243 \times 1$; i.e., $\ell = 243 \times 3$ nm and $A = 243 \times 1 \times 3^2$ nm^2), introduce the disorder cells (the density is 3%), and impose open-boundary conditions. In such a dirty system, the helical textures remain in a pinning regime even for finite β (often referred to as an extrinsic pinning regime[19,20,23]) as long as the applied electric current is below a threshold value (in the present system, $\approx 5.0 \times 10^{12}$ A m^{-2} for $\beta = 0$ and ≈ 1.5–2.0×10^{12} A m^{-2} for

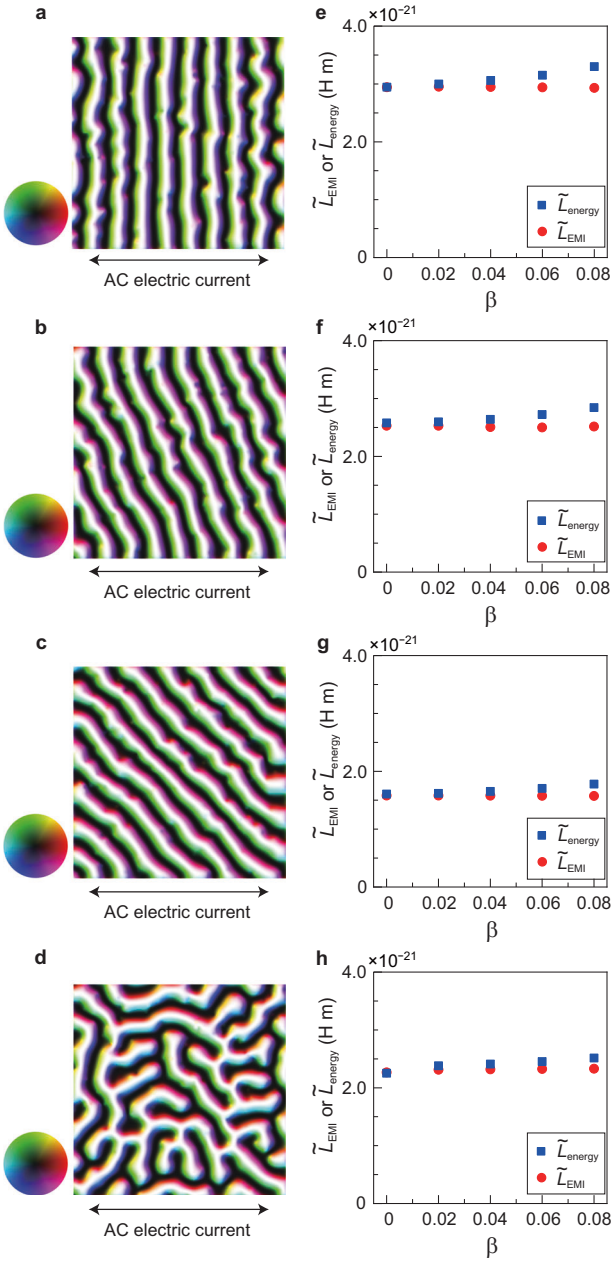

Fig. 3 Various metastable helical textures (a–d) and corresponding inductivity (e–h). The current-induced magnetic texture dynamics are calculated under the application of a weak AC current, 5.0×10^{10} A m^{-2}. This current magnitude is so weak that the current-induced deformation of the magnetic textures is not discernible in the images, but it is numerically detectable. The frequency of the AC current is 50 MHz, which is so low that the response delay of the texture deformation from the time-varying current is negligible. These conditions are satisfied for all β values we investigated in this study ($\alpha = 0.04$). To obtain the metastable helical textures at $t = 0$, a pristine helical texture with a different oblique angle of the helical $\boldsymbol{q}$-vector (for **a**–**c**) or a random spin configuration (for **d**) is prepared as an initial state and then relaxed under zero current.

finite β ($0.02 \le \beta \le 0.08$)); hence, in dirty systems, $L_{\rm EMI}$ and $L_{\rm energy}$ exhibited by the magnetic-texture dynamics in a pinned regime can be examined for both $\beta = 0$ and $\beta > 0$. Note that because of the presence of disorder, the spin texture can adopt various metastable states. Here, we show four different examples of metastable helical textures, each of which are shown in Fig. 3a–d:

The helical $\boldsymbol{q}$-vector of the three systems (Fig. 3a–c) forms approximately 0°, 20°, and 45° with the AC current direction along the horizontal direction, respectively, whereas the highly disordered helix shown in Fig. 3d has no specific $\boldsymbol{q}$-vector.

For the dirty systems, similar to the case of the clean system, we obtain $V_e(t) \propto \frac{d(Aj(t))}{dt}$ and $\Delta E(t) \propto (Aj(t))^2$; thus, $\tilde{L}_{\mathrm{EMI}}$ and $\tilde{L}_{\mathrm{energy}}$ are derived separately. Figure 3e–h summarizes the results for the four systems. We find that for all magnetic systems, $\tilde{L}_{\mathrm{EMI}} \approx \tilde{L}_{\mathrm{energy}}$ invariably holds within 2% relative error for $\beta = 0$, whereas such a good agreement is not seen for finite β. Parenthetically, among the three helical structures shown in Fig. 3a–c, the inductivity is maximized when the helical $\boldsymbol{q}$-vector is parallel to the current direction, consistent with the fact that the STT is most effective when the current is along the magnetic modulation direction.

DISCUSSION

Our numerical observations suggest that as long as a slowly varying magnetic texture in a pinned regime is considered, the limitations discussed in the Models section play a minor role at $\beta = 0$. The implications of these observations are that at $\beta = 0$, (i) the EEF can be well described by Eq. (1), which is the formalism derived in the adiabatic limit, and (ii) the EEF described by Eq. (1) is also consistent with the current-induced magnetic-texture dynamics described by Eq. (6) in terms of the energy conservation. Although there is some controversy about the physical meaning of β[26,28–31], some microscopic approaches indicate that the adiabatic limit corresponds to $\beta = 0$[26,28,30], and it was discussed[31–34] that Eq. (1) is valid only for $\beta = 0$. Our numerical observations appear to be consistent with this theoretical argument.

In the three dirty systems with a different oblique angle of the helical $\boldsymbol{q}$-vector and one highly disordered helical texture in which the $\boldsymbol{q}$-vector is ill-defined, we observe a tendency that as β increases, the agreement between $\tilde{L}_{\mathrm{EMI}}$ and $\tilde{L}_{\mathrm{energy}}$ worsens and $\tilde{L}_{\mathrm{energy}}$ becomes larger than $\tilde{L}_{\mathrm{EMI}}$; i.e., for finite β, the increase of the magnetic system energy due to current appears to exceed the work done by the external power supply, and the present framework does not conserve energy [but the relative error is still <12% at the highest β(=0.08) for the magnetic textures considered in this study]. Thus, it appears that in order to satisfy $\tilde{L}_{\mathrm{energy}} = \tilde{L}_{\mathrm{EMI}}$ at finite β, the EEF must be greater than that given by Eq. (1). In this context, we note that several theoretical studies have led to an additional correction term, $-\beta \frac{\hbar}{2|e|}(\partial_t \boldsymbol{m} \cdot \partial_i \boldsymbol{m})$, on the right-hand side of Eq. (1), that was derived using a different perspective[31–34]. However, it can be shown both analytically and numerically that adding this term further decreases $\tilde{L}_{\mathrm{EMI}}$ (Supplementary Note 2 and Fig. S1); in fact, it was the contribution of this correction term that led to the possibility of negative inductance in the previous theoretical study[12]. Thus, $\tilde{L}_{\mathrm{energy}}$ and $\tilde{L}_{\mathrm{EMI}}$ are still inconsistent, even though they should be equivalent if Eq. (2) holds. This discrepancy implies that the emergent inductance at finite β is ill-defined, at least in the present framework (see also ref. [35]). It remains a challenge for the future to establish a theoretical framework that self-consistently describes the energy and voltage response associated with the interplay between electric current and magnetic textures, especially for finite β.

Given these things, it appears also challenging to quantitatively describe the EEF, for instance, in nonslowly varying spin textures and in systems that deviate from the adiabatic limit. Nevertheless, our observations raise a new perspective on this issue; that is, for a given spin system, whether inductor behavior can emerge is equivalent to whether the system can store energy by applying an electric current. For instance, if the magnetic structure exhibits some elastic deformation under current, it is necessarily accompanied by some increase in the magnetic energy; accordingly, when the applied current is time-varying, the energy is stored or released in response to the current variations, and this behavior is equivalent to inductor. It could be said that there can be as many mechanisms for emergent inductors as there are mechanisms for storing energy by means of electric current. Thus, it would be an interesting direction to explore the emergent inductor function that is beyond the current-induced spin reorientation, which is the mechanism considered thus far. In general, the calculation of energy in a nonequilibrium steady state under current involves subtle issues, but elastic magnetic-structure deformations in a pinned regime appear to be well described by the Hamiltonian of an equilibrium system.

The energetic perspective discussed so far is a way of thinking that by no means allows for a negative inductance, even though the literature reports negative emergent inductance[10–14]. For our conclusion to be coherent, we have to explain this apparent contradiction while maintaining our standpoint that physically meaningful inductance must be positive. In this context, we emphasize that in the standard equivalent circuit analysis, the observation of negative $\mathrm{Im}\,Z(\omega)$ proportional to ω does not imply negative L, especially when $\mathrm{Re}\,Z(\omega)$ is finite: This misunderstanding about the definition of inductance is at the root of the confusion. For instance, in the previous experiments[10,11], the authors observed the following complex impedance $Z(\omega)$ at a given current density:

$$Z(\omega) = R_{\mathrm{DC}} + i\omega \frac{\eta}{1 + i\omega\tau} \quad (\eta < 0), \tag{11}$$

where the three parameters, R_{DC}, η, and τ, denote the DC resistance, a constant related with the magnitude of $\mathrm{Im}\,Z(\omega)$, and the time constant, respectively. Thus, the result, $\frac{Z(\omega)-R_{\mathrm{DC}}}{i\omega} = \frac{\eta}{1+i\omega\tau}$ with $\eta < 0$, was interpreted as the realization of negative inductance with a Debye-like frequency dependence. However, in terms of the standard equivalent circuit analysis, this $Z(\omega)$ [Eq. (11)] is fully reproduced by an equivalent circuit shown in Fig. 4, which is comprised of three positive-valued elements, R_a, R_b, and C, that are chosen to satisfy $R_a + R_b = R_{\mathrm{DC}}$, $CR_b = \tau$, and $CR_b^2 = -\eta > 0$. Thus, the observation of Eq. (11)-type $Z(\omega)$ with negative η is usually interpreted as the indication of a stray capacitance involved in the circuit, rather than a superficial negative inductance. In fact, we experimentally find that within a microfabricated sample, the system exhibits a background signal of $\frac{\mathrm{Im}\,Z(\omega)}{\omega} \approx -400$ nΩ s, which superficially corresponds to a (fictitious) negative inductance, ≈ −400 nH (for details, see Supplementary Note 3 and Fig. S2). Considering that the elimination of the background is generally not straightforward, it should be noted that $\mathrm{Im}\,Z(\omega)$ in the experiment is prone to be affected by this relatively large negative-L-like signal.

To conclude, we propose an energetic definition of the self-inductance coefficient, L, in the low-frequency regime for so-called emergent inductors and investigate its validity numerically for the case of helical magnetic textures in a pinned regime. The inductance defined from the energy increase of the magnetic system under current and that from the emergent electric field are found to agree with each other within the numerical errors, especially for the case of slowly varying spin textures and $\beta = 0$. Although our numerical approach appears to be less justified for finite β and nonslowly varying spin textures, we conclude that the

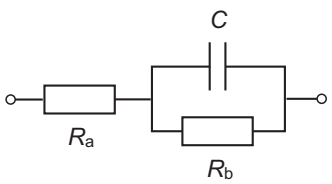

Fig. 4 An equivalent circuit that can reproduce superficial negative inductance with Debye-like frequency dispersion, $\boldsymbol{Z(\omega) = R_{DC} + i\omega \frac{\eta}{1+i\omega\tau}}$ with $\boldsymbol{\eta < 0}$. The $Z(\omega)$ can be reproduced by choosing $R_a(>0)$, $R_b(>0)$, and $C(>0)$ to satisfy $R_a + R_b = R_{\mathrm{DC}}$, $CR_b = \tau$, and $CR_b^2 = |\eta|$.

main concept of inductors in which energy is stored and released under a time-varying electric current should hold for any spin-based inductor. Conversely, if a magnetic system is capable of storing energy under current by changing the magnetic texture, the system potentially behaves as an inductor. Toward a microscopic understanding of emergent inductors, a comprehensive consideration of not only the emergent electric field but also energy will be important. Additionally, the emergent electric field beyond the linear response regime is an interesting subject, which may be more relevant to the experiments reported thus far.

DATA AVAILABILITY

The data used in this work are available from the corresponding author upon reasonable request.

Received: 14 July 2023; Accepted: 25 October 2023;
Published online: 22 November 2023

REFERENCES

1. Slonczewski, J. C. Current-driven excitation of magnetic multilayer. *J. Magn. Magn. Mater.* **159**, L1–L7 (1996).
2. Berger, L. Emission of spin waves by a magnetic multilayer traversed by a current. *Phys. Rev. B* **54**, 9353–9358 (1996).
3. Yamanouchi, M., Chiba, D., Matsukura, F. & Ohno, H. Current-induced domain-wall switching in a ferromagnetic semiconductor structure. *Nature* **428**, 539–542 (2004).
4. Volovik, G. E. Linear momentum in ferromagnets. *J. Phys. C* **20**, L83–L87 (1987).
5. Barnes, S. E. & Maekawa, S. Generalization of Faraday's law to include non-conservative spin forces. *Phys. Rev. Lett.* **98**, 246601 (2007).
6. Yang, S. A. et al. Universal electromotive force induced by domain wall motion. *Phys. Rev. Lett.* **102**, 067201 (2009).
7. Zang, J., Mostovoy, M., Han, J. H. & Nagaosa, N. Dynamics of skyrmion crystals in metallic thin films. *Phys. Rev. Lett.* **107**, 136804 (2011).
8. Schulz, T. et al. Emergent electrodynamics of skyrmions in a chiral magnet. *Nat. Phys.* **8**, 301–304 (2012).
9. Nagaosa, N. Emergent inductor by spiral magnets. *Jpn. J. Appl. Phys.* **58**, 120909 (2019).
10. Yokouchi, T. et al. Emergent electromagnetic induction in a helical-spin magnet. *Nature* **586**, 232 (2020).
11. Kitaori, A. et al. Emergent electromagnetic induction beyond room temperature. *Proc. Natl Acad. Sci. USA* **118**, e2105422118 (2021).
12. Ieda, J. & Yamane, Y. Intrinsic and extrinsic tunability of Rashba spin–orbit coupled emergent inductors. *Phys. Rev. B* **103**, L100402 (2021).
13. Kurebayashi, D. & Nagaosa, N. Electromagnetic response in spiral magnets and emergent inductance. *Commun. Phys.* **4**, 260 (2021).
14. Kitaori, A. et al. Doping control of magnetism and emergent electromagnetic induction in high-temperature helimagnets. *Phys. Rev. B* **107**, 024406 (2023).
15. Nattermann, T., Shapir, Y. & Vilfan, I. Interface pinning and dynamics in random systems. *Phys. Rev. B* **42**, 8577–8586 (1990).
16. Chauve, P., Giamarchi, T. & Doussal, P. L. Creep and depinning in disordered media. *Phys. Rev. B* **62**, 6241–6267 (2000).
17. Kleemann, W. Universal domain wall dynamics in disordered ferroic materials. *Annu. Rev. Mater. Res.* **37**, 415–448 (2007).
18. Tatara, G. & Kohno, H. Theory of current-driven domain wall motion: spin transfer versus momentum transfer. *Phys. Rev. Lett.* **92**, 086601 (2004).
19. Thiaville, A., Nakatani, Y., Miltat, J. & Suzuki, Y. Micromagnetic understanding of current-driven domain wall motion in patterned nanowires. *Europhys. Lett.* **69**, 990–996 (2005).
20. Tatara, G. et al. Threshold current of domain wall motion under extrinsic pinning, β-term and non-adiabaticity. *J. Phys. Soc. Jpn.* **75**, 064708 (2006).
21. Koyama, T. et al. Observation of the intrinsic pinning of a magnetic domain wall in a ferromagnetic nanowire. *Nat. Mat.* **10**, 194–197 (2011).
22. Tatara, G., Kohno, H. & Shibata, J. Microscopic approach to current-driven domain wall dynamics. *Phys. Rep.* **468**, 213–301 (2008).
23. Burrowes, C. et al. Non-adiabatic spin-torques in narrow magnetic domain walls. *Nat. Phys.* **6**, 17–21 (2010).
24. Iwasaki, J., Mochizuki, M. & Nagaosa, N. Universal current-velocity relation of skyrmion motion in chiral magnets. *Nat. Commun.* **4**, 1463 (2013).
25. Jackson, J. D. *Classical Electrodynamics* 3rd edn (Wiley, 1998).
26. Zhang, S. & Li, Z. Roles of nonequilibrium conduction electrons on the magnetization dynamics of ferromagnets. *Phys. Rev. Lett.* **93**, 127204 (2004).
27. Vansteenkiste, A. et al. The design and verification of MuMax3. *AIP Adv.* **4**, 107133 (2014).
28. Barnes, S. E. & Maekawa, S. Current-spin coupling for ferromagnetic domain walls in fine wires. *Phys. Rev. Lett.* **95**, 107204 (2005).
29. Kohno, H., Tatara, G. & Shibata, J. Microscopic calculation of spin torques in disordered ferromagnets. *J. Phys. Soc. Jpn.* **75**, 113706 (2006).
30. Duine, R. A. Spin pumping by a field-driven domain wall. *Phys. Rev. B* **77**, 014409 (2008).
31. Tserkovnyak, Y. & Mecklenburg, M. Electron transport driven by nonequilibrium magnetic textures. *Phys. Rev. B* **77**, 134407 (2008).
32. Duine, R. A. Effects of nonadiabaticity on the voltage generated by a moving domain wall. *Phys. Rev. B* **79**, 014407 (2009).
33. Shibata, J. & Kohno, H. Spin and charge transport induced by gauge fields in a ferromagnet. *Phys. Rev. B* **84**, 184408 (2011).
34. Yamane, Y. & Ieda, J. Skyrmion-generated spin motive forces in inversion broken ferromagnets. *J. Magn. Magn. Mater.* **491**, 165550 (2019).
35. Furuta, S., Koshibae, W. & Kagawa, F. Symmetry of the emergent inductance tensor exhibited by magnetic textures. npj Spintronics https://doi.org/10.1038/s44306-023-00001-4 (2023).

ACKNOWLEDGEMENTS

The authors thank Y. Liu, S. Maekawa, N. Nagaosa, and G. Tatara for their valuable discussions. S.F. and F.K. thank A. Kikkawa for providing MnSi crystals. This work was partially supported by JSPS KAKENHI (Grants Nos. 20K03810, 18H05225, 21H04442, and 23K03291), JST CREST (Grants Nos. JPMJCR1874 and JPMJCR20T1), and the JSPS Summer Program 2020, who funded S.H.M.'s placement at RIKEN, Japan.

AUTHOR CONTRIBUTIONS

S.F., S.H.M. and K.K. conducted the numerical calculations. S.F. analyzed the data and conducted the analytic calculation. S.F. and F.K. conducted the experiments on MnSi. F.K. conceived the project and wrote the draft with S.F. and W.K. All the authors discussed the results and commented on the manuscript.

COMPETING INTERESTS

The authors declare no competing interests.

ADDITIONAL INFORMATION

Supplementary information The online version contains supplementary material available at https://doi.org/10.1038/s44306-023-00004-1.

Correspondence and requests for materials should be addressed to Fumitaka Kagawa.

Reprints and permission information is available at http://www.nature.com/reprints

Publisher's note Springer Nature remains neutral with regard to jurisdictional claims in published maps and institutional affiliations.